AGU PUBLICATIONS

Geochemistry, Geophysics, Geosystems

RESEARCH ARTICLE
10.1002/2017GC007250

Key Points:
- Sediment grain-size is controlled by IRD input and bottom current strength
- The AABW formation rate was enhanced during glacial terminations
- The bottom current strength and AABW formation rate affect deep Southern Ocean carbon storage

Supporting Information:
- Supporting Information S1
- Data Set S1
- Data Set S2

Correspondence to:
L. Wu,
wuli@tongji.edu.cn;
R. Wang,
rjwang@tongji.edu.cn

Citation:
Wu, L., Wang, R., Xiao, W., Krijgsman, W., Li, Q., Ge, S., & Ma, T. (2018). Late quaternary deep stratification-climate coupling in the Southern Ocean: Implications for changes in abyssal carbon storage. *Geochemistry, Geophysics, Geosystems*, *19*, 379–395. https://doi.org/10.1002/2017GC007250

Received 22 SEP 2017
Accepted 4 JAN 2018
Accepted article online 17 JAN 2018
Published online 3 FEB 2018

Late Quaternary Deep Stratification-Climate Coupling in the Southern Ocean: Implications for Changes in Abyssal Carbon Storage

Li Wu[1], Rujian Wang[1], Wenshen Xiao[1], Wout Krijgsman[2], Qianyu Li[1,3], Shulan Ge[4], and Tong Ma[1]

[1]State Key Laboratory of Marine Geology, Tongji University, Shanghai, China, [2]Department of Earth Sciences, Utrecht University, Utrecht, the Netherlands, [3]School of Earth and Environment Sciences, University of Adelaide, SA, Australia, [4]State Oceanic Administration, First Institute of Oceanography, Qingdao, China

Abstract The Southern Ocean plays an important role in modulating Pleistocene atmospheric CO_2 concentrations, but the underlying mechanisms are not yet fully understood. Here, we report the laser grain-size distribution and Mn geochemical data of a 523 kyr-long sediment record (core ANT30/P1-02 off Prydz Bay; East Antarctica) to trace past physical changes in the deep Southern Ocean. The core sediments are predominantly composed of clay and silt-sized material. Three grain size end-members (EM) as well as three sensitive grain size classes (SC) were discerned, interpreted as Ice Rafted Debris (EM1 and SC1), and coarse (EM2 and SC2) and fine (EM3, SC3) materials deposited from bottom nepheloid layers, respectively. Ratios of EM2/(EM2 + EM3) and SC2/SC3 reveal changes in the local bottom current strength, which is related to the deep ocean diapycnal mixing rate, showing higher values during interglacial periods and lower values during glacial periods. MnO was enriched at each glacial termination, probably caused by abrupt elevations in Antarctic bottom water (AABW) formation rate. Lower AABW formation rate and reduced deep diapycnal mixing during glacial periods enhanced deep Southern Ocean stratification, contributing to glacial atmospheric CO_2 drawdown. The elevated AABW formation and enhanced deep diapycnal mixing during glacial terminations alleviated such deep stratification, promoting deeply sequestered CO_2 to outgas.

Plain Language Summary The Southern Ocean is a key place to modulate atmospheric CO_2 concentrations on different timescales. This article demonstrates that the deep stratification of the Southern Ocean was enhanced during glacial periods, thereby contributing to glacial atmospheric CO_2 drawdown, while this deep stratification was alleviated during glacial terminations, and thus deeply sequestered CO_2 in the Southern Ocean can outgas into the atmosphere.

1. Introduction

Atmospheric CO_2 plays a critical role in triggering glacial cycles by amplifying the impact of orbitally modulated insolation and ice sheet dynamics (Abe-Ouchi et al., 2013; Shakun et al., 2012; Timmermann et al, 2009). The ocean interior has long been considered as the major agent modulating atmospheric CO_2 concentrations due to its great capability of storing carbon (Abelmann et al., 2015; Adkins et al., 2002; Ferrari et al., 2014; Sigman & Boyle, 2000; Sikes, 2012; Toggweiler et al., 2006; Watson & Naveira Garabato, 2006). Particularly, the Southern Ocean is recognized as the key area where atmospheric/oceanic CO_2 exchange occurs (Jaccard et al., 2013; Marshall & Speer, 2012; Schmitt et al., 2012; Sigman et al., 2010) because it represents the upwelling branch of the Meridional Overturning Circulation (MOC) (Marshall & Speer, 2012).

A series of physical, chemical, and biological processes are involved in the atmospheric/oceanic CO_2 exchanges (e.g., Abelmann et al., 2006; Elderfield & Rickaby, 2000; Ferrari et al., 2014; Frank et al., 2000; Jaccard et al., 2016; Jaccard & Galbraith, 2012; Moore et al., 2000; Schneider-Mor et al., 2005; Sigman & Boyle 2000; Stephens & Keeling, 2000). Box model simulations used to explain past CO_2 variability assume that the atmospheric CO_2 is determined by the net rate of CO_2 exchange between the ocean and the atmosphere (e.g., Brovkin et al., 2007; Hain et al., 2010; Knox & McElroy, 1984; Sarmiento & Toggweiler, 1984; Watson & Naveira Garabato, 2006). The net exchange is determined by the difference between the

"biological pump," which brings CO_2 from the ocean surface water and atmosphere into the deep ocean (Galbraith & Jaccard, 2015; Jaccard et al., 2013, 2016), and physical ocean ventilation, which leads deeply sequestered CO_2 to outgas in the Southern Ocean. Either increasing biological productivity, or decreasing the exchange of water between the surface and depth, can decrease the atmospheric CO_2 concentration (e.g., Jaccard et al., 2013).

Elevated productivity in the Southern Ocean was previously considered to be the predominant reason for the atmosphere CO_2 drawdown during glacial periods (Knox & McElroy, 1984; Kumar et al., 1995; Sarmiento & Toggweiler, 1984). This viewpoint, however, was challenged by observations that two different modes of export-production changes exist in the Southern Ocean, resulting in seesaw-like temporal patterns across the Antarctic Polar Front (APF) (Jaccard et al., 2013). Reduction in export production north (south) of the APF is accompanied by elevation in export production south (north) of APF (vice versa) (Jaccard et al., 2013), implying that the total export production in the Southern Ocean did not significantly change over glacial-interglacial variations, as has been registered in ice core $nssSO_4^{2-}$ (nonsea-salt sulfate) records (Wolff et al,. 2006, 2010).

Large-scale vertical circulation changes in the Southern Ocean are mainly determined by the MOC that consists of an upper and a lower circuit (Marshall & Speer, 2012). The upper circuit is fed by the formation processes of North Atlantic Deep Water (NADW) and by deep diapycnal upwelling, while the lower circuit is fed by the formation of Antarctic bottom water (AABW). The AABW is the coldest and densest water in the global ocean and forms in the Weddell Sea (Foldvik et al., 2004; Foster & Carmack, 1976), Ross Sea (Whitworth & Orsi, 2006), and some other Antarctic coastal areas including the Adelie Land region (Williams et al., 2008) and the Prydz Bay region (Ohshima et al., 2013; Yabuki et al., 2006). Box model simulations (e.g., Brovkin et al., 2007; Hain et al., 2010) and geological archive studies (e.g., Anderson et al., 2009, 2014; Jaccard et al., 2013; Martínez-García et al., 2014; Tang et al., 2016; Wu et al., 2017) focusing on the upper circuit demonstrated that atmospheric CO_2 drawdown in glacial time was associated with enhanced surface stratification and/or sea ice cover in combination with an elevated dust-borne iron fertilization in the Southern Ocean, while the deglacial elevation in atmospheric CO_2 was pertinent to enhanced wind-driven deep water upwelling (Anderson et al., 2009; Toggweiler et al., 2006). Studies directly associated with the lower circuit mainly dealt with proxies for bottom water redox state (Galbraith & Jaccard, 2015; Jaccard et al., 2016; Jaccard & Galbraith, 2012; Wagner & Hendy, 2017). These studies show a significant change in the bottom water redox state within the last glacial cycle, with the bottom water being anoxic during the glacial and well oxygenated during the deglaciation, indicating a drastic change in the deep ocean ventilation across the last glacial terminations, consistent with model simulations (Jaccard et al., 2016), radiocarbon analysis on paired planktonic and benthic foraminifera (Skinner et al., 2010), and deep sea corals (Burke & Robinson, 2012) as well as ice core registered carbon isotope changes in atmopsheric CO_2 ($\delta^{13}C_{atm}$) (Schmitt et al., 2012). The forcing mechanisms causing these physical changes over past glacial-interglacial variations in the Southern Ocean are, however, still unclear. Longer (beyond the last glacial cycle) geological archives focusing on the lower MOC circuit are necessary to better understand the role of Southern Ocean in modulating past atmospheric CO_2 variability.

Here we aim to investigate the changes in circulation and ventilation of the deep Southern Ocean and their link to atmosphere-ocean carbon cycling. For this purpose, we determine the grain-size distributions (GSDs) as well as the bulk sediment Manganese (Mn) geochemistry of a gravity sediment core (ANT30/P1–02) retrieved off Prydz Bay (East Antarctica). Previous work on this core focused on productivity-climate coupling and established a robust time frame back to 523 ka (Wu et al., 2017). Grain size of terrigenous sediments is a sensitive parameter preserving information on provenance, transport, and sedimentation processes (Jonkers et al., 2009; McCave & Hall, 2006). Grain size of abyssal sediments at high latitudes is often used to monitor variations in abyssal current strength (e.g., Lamy et al., 2015; McCave et al., 2014; Prins et al., 2002; Pudsey, 1992). Redox sensitive elements in marine sediments can register the redox variations in bottom water masses (Galbraith & Jaccard, 2015; Jaccard et al., 2016; Jaccard & Galbraith, 2012; Wagner & Hendy, 2017). Taking Mn for example, it is typically enriched in well-oxygenated sediments as Mn (IV), while it dissolves and diffuses under anoxic/reducing conditions as Mn (II) (Galbraith & Jaccard, 2015; Jaccard & Galbraith, 2012; Jaccard et al., 2016; Mangini et al., 2001; Presti et al., 2011). A combination of grain size and Mn geochemistry of abyssal sediments may thus shed light on changes in deep ocean circulation and ventilation history.

In summary, this study aims to (1) discern the predominant factors affecting the GSDs and Mn geochemistry in the sediments; (2) investigate the changes in the bottom current strength and deep ventilation over the past glacial-interglacial changes; and (3) discuss the link between the glacial-interglacial physical changes in the deep Southern Ocean and the abyssal carbon storage.

2. Regional Environmental and Geological Setting

Prydz Bay is the third largest embayment around Antarctica (Figure 1). It is situated between 65°E and 80°E at the seaward terminus of a major Mesozoic graben structure, the Lambert Graben, which is now occupied by the Lambert Glacier and the Amery Ice Shelf system (LGAISS) (Passchier et al., 2003). The LGAISS system is the largest outlet glacier system on Antarctica, draining 16–20% of the East Antarctic ice into the Southern Ocean (Hannah, 2006).

The ocean current system around Prydz Bay is composed of five branches (Figure 1b) (Bindoff et al., 2000; Cooper & O'Brien, 2004; Vaz & Lennon, 1996). The Antarctic Coastal Current (CoC) flows westward, bringing in cold waters from the east. The Antarctic Slope Current (ASC), driven by Southern Easterly Wind (SEW)

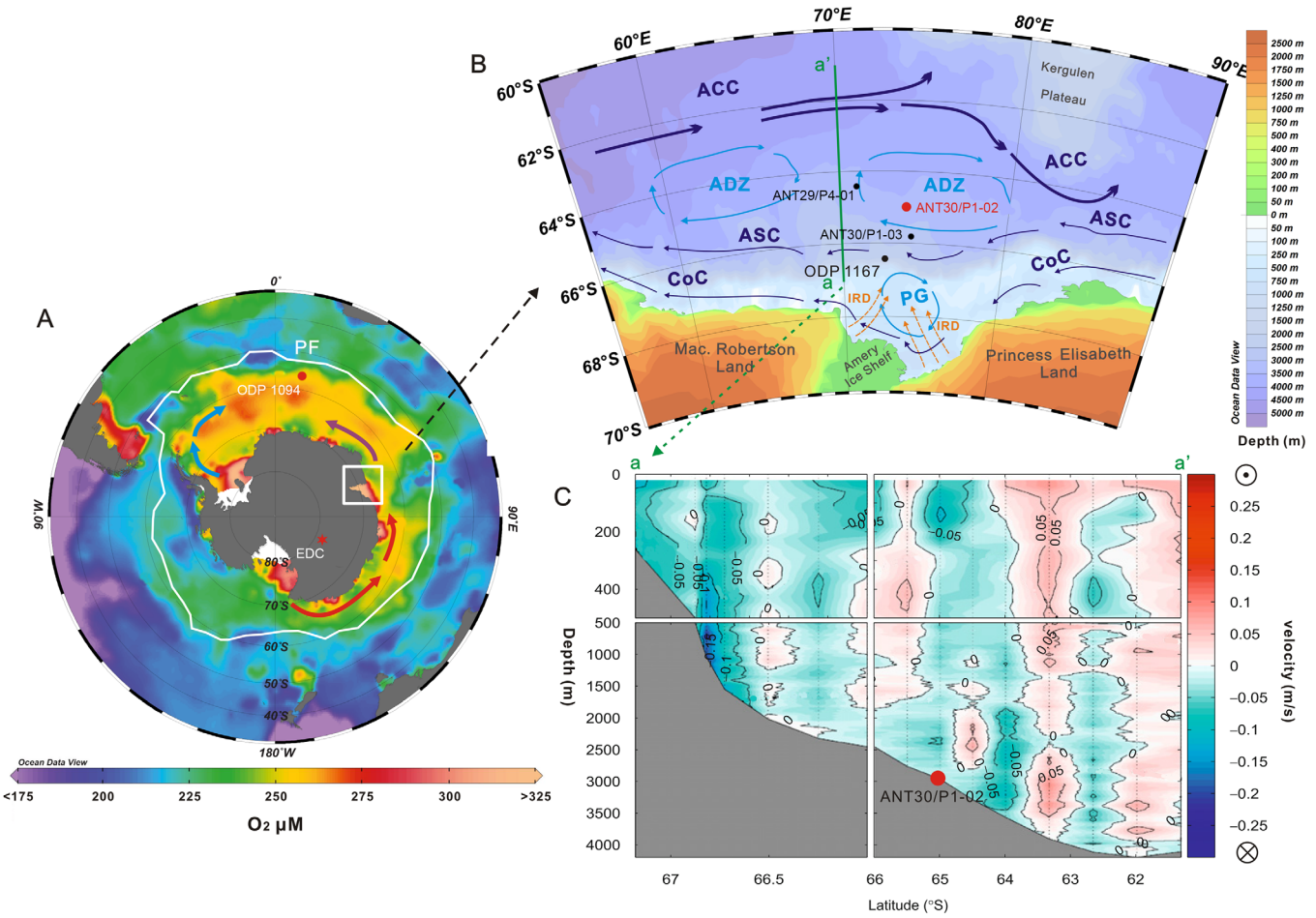

Figure 1. (a) Dissolved oxygen concentrations in bottom waters of the modern Southern Ocean (Garcia et al., 2009), modified after Jaccard et al. (2016). The Prydz Bay region is indicated by a white box. PF: Antarctic Polar Front. EDC: EPICA Dome C ice core site (EPICA Community Members, 2004). Arrows with red, purple, and celeste colors indicate major flow paths of AABW of Ross Sea plus Adele Land, Prydz Bay, and Weddell Sea origins, respectively according to Williams et al. (2008) and Meijers et al. (2010). (b) Core site and environmental settings of the Prydz Bay region. IRD: tracks of Ice Rafted Debris. CoC: Antarctic Coastal Current. PG: Prydz Gyre. ASC: Antarctic Slope Current. ADZ: Antarctic Divergence Zone. ACC: Antarctic Circumpolar Current. IRD tracks and current system are based on Cooper and O'Brien (2004), Forsberg et al. (2008), and Meijers et al. (2010). The sites of ANT30/P1–03 and ANT29/4-01 are from Wu et al. (2017). ODP site 1167 is from Theissen et al. (2003). The topographic map is generated using Ocean Data View version 4.6.5 (Schlitzer, 2009). (c) Vertical profile section of LADCP zonal velocities (m/s) at 70°E (a-a' profile in Figure 1b) in the Prydz Bay region is modified after (Meijers et al., 2010). Positive and negative values are eastward and westward velocity, respectively. Scale changes are indicated by the breaks in the axis. The P1-2 core site is represented as a red-filled circle.

stress, also flows from east to west but over the continental slope (Mathiot et al., 2011). Between the CoC and the ASC, the clockwise rotating Prydz Gyre (PG) mainly flows over the continental shelf. North of the ASC, the cyclonic Antarctic Divergence Zone (ADZ) represent a series of mesoscale eddies forming under the shear stress of the Southern Westerly Wind (SWW) and Southern Easterly Wind (SEW). It can intrude into the shelf and bring up the relatively warm and salty Antarctic Deep Water (Yabuki et al., 2006). Further offshore, the northern Antarctic Circumpolar Current (ACC) flows eastward and connects the Southern Ocean with other oceans. A vertical profile of current velocity distributions (during summer) derived from Lowered Acoustic Doppler Current Profiler (LADCP) shows westward ASC and eastward ACC intertwine with each other between 66.5° and 62°S (Figure 1c) (Meijers et al., 2010).

In the Prydz Bay area, shelf waters with low temperature (close to their freezing points) and varying salinities comprise the major water masses over the shelf (Nunes Vaz & Lennon, 1996; Smith et al., 1984). Off the bay, the relatively warm ($T > 1°C$) and salty ($S > 34.65$ psu) Circumpolar Deep Water (CDW) accounts for the major part of the water mass (Meijers et al., 2010). Below the CDW are two types of AABWs (Meijers et al., 2010): one forms in the west of Prydz Bay by local shelf processes and deep convection (Meijers et al., 2010; Ohshima et al., 2013), the other is a mixture derived from the Ross Sea and Adelie Land and enters the region from the east (Bindoff et al., 2000; Meijers et al., 2010; Williams et al., 2008).

Modern summer sea ice distribution is confined to the inner Prydz Bay. Modern winter sea ice can expand to the midline between the modern APF and the Prydz coastline (~58°S). During the Last Glacial Maximum (LGM), the winter sea ice limit had advanced to the position of the modern APF (~51°S), while the summer sea ice limit during the LGM is considered to be similar to its modern position (Crosta et al., 1998a, 1998b; Gersonde et al., 2005; Röthlisberger et al., 2010), or to have expanded to the modern winter sea ice limit (Goosse et al, 2013).

3. Materials and Methods

3.1. Material

Gravity core ANT30/P1-02 (hereafter, P1-2) was retrieved off Prydz Bay (72.94°E; 65.01°S; 2916 m water depth; 6.24 m core length) during the 30th Chinese Antarctica Expedition onboard R/V *Xuelong* in 2013–2014. The color of the core varies between olive, brown, and gray. According to wet and dry sieving experiments, the core sediments principally consist of structureless clayey silt with minor proportion of sand (63–2000 μm) and a few randomly distributed drop stones (>2 mm). No significant bioturbations were found all through the core. The core site is adjacent to the Prydz Bay AABW production region (Meijers et al., 2010; Ohshima et al., 2013; Yabuki et al., 2006), and is on the flow route of AABW from the Ross Sea and Adelie Land region. It is furthermore under the influence range of the ADZ, thus representing an ideal place to trace past changes in the strength of AABW formation and the deep circulation in the ADZ.

3.2. Analytical Methods

A total of 312 subsamples were taken at 2 cm intervals from the core and dried at 40°C for further analysis.

For Mn and Al analysis, the dry bulk sediment samples were finely ground, and ashed at 600°C for 2 h to measure the loss of ignition. The sediment samples, together with a series of Chinese and USGS rock and sediment standards, were treated with a concentrated $HF + HNO_3$ mixture, and were measured by ICP-OES (IRIS Advantage) (Wei et al., 2003). The relative standard deviation (RSD), which was calculated from standard reference materials, is generally better than 2%. Duplicate measurements on randomly selected parallel sample pairs indicate a very good reproducibility (RSD < 3%).

For grain-size analysis, 0.15 g of dry bulk sediment from each sample was successively treated with 10% H_2O_2, 1.0 *N* HCl, and 2.0 *N* NaOH to remove organic carbon, carbonate, and biogenic silica in a water bath at 85°C. The treated samples, after confirmation of successful removal of all biogenic constituents by microscope inspection, were soaked with 20 mL distilled water and dispersed by a ultrasonator for 2 min, followed by analysis with a Coulter Automatic Laser Analyzer (Beckman Coulter LS230). The particle Size Analyzers can be used for grain size analysis in the range 0.375–2,000 μm. The analytical reproducibility was assessed here with the normalized Euclidian distance (ND) according to Roberson and Weltje (2014). Measurements on 30 randomly selected duplicate samples indicate the NDs are all less than 0.02 (2%), indicating the reproducibility is very good.

All analyses were carried out in the State Key Laboratory of Marine Geology, Tongji University.

3.3. Data Processing

To measure the extent of authigenic Mn enrichment in the sediments, we calculated the enrichment factor of Mn according to Nolting et al. (1999) as follow

$$EF(Mn) = (Mn/Al)_{sample}/(Mn/Al)_{shale} \quad (1)$$

where EF(Mn) is the enrichment factor of Mn; the $(Mn/Al)_{sample}$ and $(Mn/Al)_{shale}$ are Mn/Al ratios of the samples and shale standard, respectively. Shale standard used in this study is from Turekian and Wedepohl (1961). The Mn enrichment factor gives definite quantities about how many times excess Mn is enriched in the sediments relative to the detrital background.

Sensitive grain size classes were defined after Boulay et al. (2003) by calculating the standard deviations of each grain size interval. This is a simple but effective graphic method to determine the systematic variations in a grain size data set (Boulay et al., 2003).

The End-Member Modeling Algorithm (EMMA) was applied to the grain-size data set following the procedure described by Weltje (1997) using a software programmed by Seidel and Hlawitschka (2015). EMMA is an inversion algorithm aimed at the construction of physical (linear) mixing models, which express the input data as mixtures of a limited number of end-members with realistic compositions (Weltje, 1997). It has proven to be a powerful tool for decomposing grain-size distributions that are composed of sediment end-members from a variety of geological settings (e.g., Prins & Weltje, 1999, Prins et al., 2000; Stuut et al., 2002).

Prior to EMMA calculation, data columns at the coarse end (340–2,000 μm) were amalgamated as one column because they are dominated by zero values. Percentiles of 5 and 95 were selected to be the weights after several trials to obtain a better estimation of the linear mixing part in the raw data set. At last, all the samples ($n = 312$) of 72 grain-size intervals from 0.4 to 340 μm were put in the program (Seidel & Hlawitschka, 2015) for EMMA calculation.

4. Age Model

Poor preservation of carbonates at high latitudes of Southern Ocean limits application of the widely used oxygen isotope stratigraphic method to construct sediment age models (Wu et al., 2017; Xiao et al., 2016). In a recent study (Wu et al., 2017), the temporal distribution patterns of export production represented as EP derived from X-ray Fluorescence (XRF) geochemical scanning of sediment cores from Prydz Bay were found to be closely coupled with global climate change patterns recorded in LR04-$\delta^{18}O$ stack (Lisiecki & Raymo, 2005) on orbital timescales. This coupling provides an alternative way to construct age models for these sediment cores. The age model of core P1-2 used here was derived from Wu et al. (2017). According to the tuned age model, the P1-2 core spans the last 523 kyrs, with an average sedimentation rate of 1.19 cm/kyr.

5. Results

5.1. Manganese Geochemistry

MnO content varies between 0.074 and 0.617 wt. %, showing several significant pulses primarily at deglacial periods, corresponding to decreasing global ice volume (Lisiecki & Raymo, 2005) and elevated local export production (Wu et al., 2017) (Figure 2). The enrichment factor of MnO varies between 0.76 and 7.14 (Figure 2). It shares a similar distribution pattern with MnO content, with significant enrichments at every glacial termination and values approaching to the detrital background during the remaining time intervals.

5.2. Grain Size

The core sediments are primarily composed of clay and silt, except for two sand-rich layers around MIS 10/11 and MIS 12/13 (Figure 2). The grain-size distribution patterns vary in a wide range, showing two grain size modes at 2 and 300 μm respectively, while the mean distribution only presents a plateau at 1–6 μm (Figure 3a). To determine the major factors controlling the sediment grain-size distributions, we first conducted a sensitive grain-size analysis over all the grain-size intervals. In the plot of standard deviation against the grain-size intervals (Figure 3b), three major peaks with higher standard deviations at 101–494

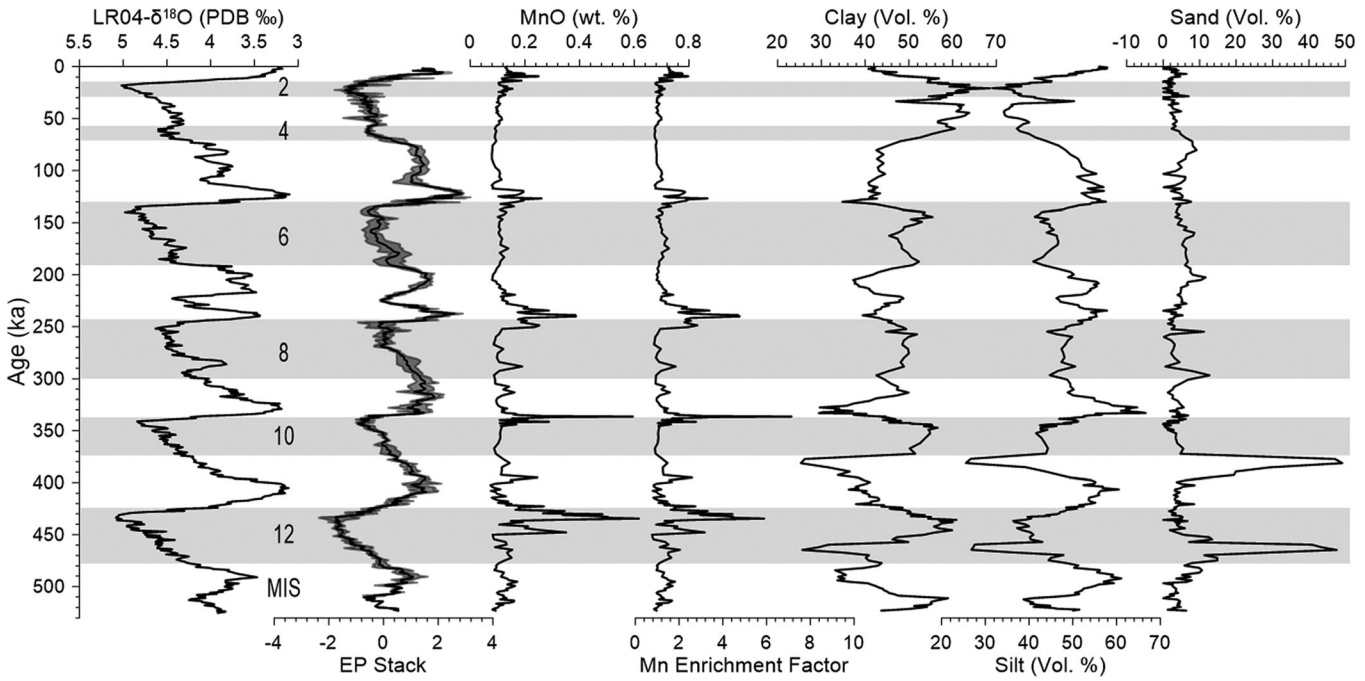

Figure 2. Temporal distributions of MnO, Mn Enrichment Factor, clay content, silt content, and sand content in ANT30/P1-02 core sediments. Also shown on the left are the LR04 benthic stack (Lisiecki & Raymo, 2005) and the EP Stack from Wu et al. (2017), representing the local export production variation pattern (EP) in the Prydz Bay region calculated from ANT30/P1–03, ANT30/P1–02, and ANT29/P4-01 (Figure 1b). The gray shade behind the EP stack curve denotes the variation range of the local EP.

μm (SC1), 9.82–27.4 μm (SC2), and 1.52–2.92 μm (SC3), can be clearly discerned as sensitive grain size classes, implying three major factors may have controlled the sediment grain-size distributions. To further determine what these factors are, we conducted an EMMA analysis on the grain-size data set. Figure 3c shows the coefficients of determination (R^2) plotted against grain size for models with 2–10 EMMA-derived end-members. The mean coefficient of determination of the grain size classes increases when the number of end-members increases (Figure 3d). The two-end-member model (R^2_{mean} = 0.51) shows low R^2 (<0.6) for the size ranges 5–20 μm and > 36 μm, while the three-end-member model (R^2_{mean} =0.78) shows low R^2 for the size range 36–121 μm only (Figure 3c). This coarse fraction can be well reproduced by models with four or more end-members. To determine the geologically suitable number of end-members, however, the coarse end (36–121 μm) can be ignored because it comprises only a small average volume fraction (~5 vol. %) of the samples (Figure 3a) and the precision at the coarse end is often lower than for the fine fraction (Jonkers et al., 2015). The grain-size range < 20 μm, to the contrary, should be well reproduced by the mixing model because this size range contains a considerable proportion of the sediment mass (e.g., Stuut et al., 2002). The goodness-of-fit statistics thus demonstrate that the three-end-member model provides the best compromise between the number of end-members and R^2, and this is also apparently consistent with the three sensitive grain size intervals (Figure 3e).

The grain-size distribution patterns of the three end-members (Figure 3e) demonstrate that EM1 is characterized by a flat distribution pattern with the poorest sorting (2.71) among the three end-members (Table 1). The coarsest sensitive grain size class SC1 (>101 μm) overlaps with the coarse end of this end-member. EM2 contains two modes at 12 and 120 μm, with the one at 12 μm being the major mode. The sorting of EM2 is the best (1.32). The sensitive grain-size class SC2 (9.82–27.4 μm) features the peak grain-size interval in EM2. EM3 shows its major mode at ~2 μm, although secondary modes at 17, 44, and 92 μm are also present. The sorting of EM3 is 1.59. The sensitive grain-size class SC3 (1.52–2.92 μm) features the major peak grain size range of EM3. In addition, it is obvious that there is an overlap between EM2 and EM3 (between 2 and 30 μm), while the sensitive grain size classes SC2 and SC3 largely bypass this overlap.

The temporal distributions of the three end-members (EM1 to EM3) are generally consistent with those of the three sensitive grain size classes (SC1–SC3) (Figure 4). EM1 and SC1 vary between 0 and 100% and between 0 and 40.9%, presenting higher values predominantly at each interglacial-to-glacial transition

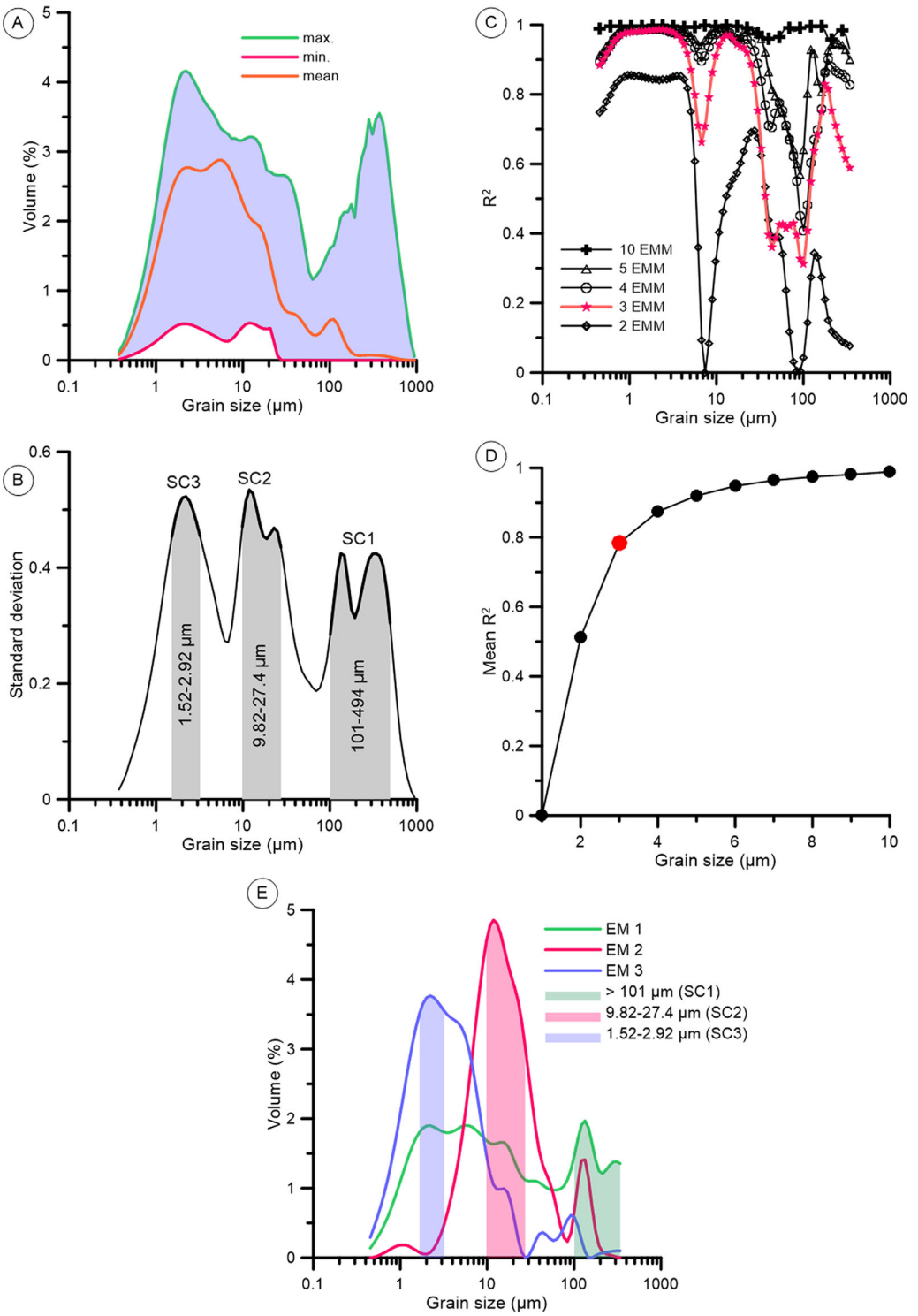

Figure 3. End-member analysis on the core sediments grain-size distributions. (a) A summary of the grain-size distributions (n = 312), including the maximum, mean, and minimum distributions and distribution range (pale blue shade) in each grain size class. (b) A plot of standard deviations of grain size frequencies against grain size class. The three sensitive grain size classes are numbered as SC1, SC2, and SC3 and indicated by pale shades (c) Coefficients of determination (R^2) for each grain size class of models with 2–10 EMMA-derived end-members. (d) Mean coefficient of determination (Mean R^2) of all grain size classes for each end-member model. The three-end-member model was selected as the best one to interpret the grain size data set and is thus highlighted by a red color. (e) Grain-size distributions of the modeled end-members from the selected three-end-member model. The colored shades highlight the three sensitive grain size classes as denoted in the legends.

Table 1
Summary of Key Statistics of the Grain-Size Distributions of EMMA-Derived End-Members

	Mean (μm)	Median (μm)	Std.	CV	Sorting	Skewness	Kurtosis
EM1	55.1	11.6	4.22	153	2.71	−0.39	0.49
EM2	27.7	15.3	13.3	131	1.32	−0.80	0.43
$EM2_{major}$	18.0	14.1	28.2	73.9	1.04	−1.28	0.31
EM3	10.3	3.32	36.2	274	1.59	−0.94	0.39
$EM3_{major}$	4.5	3.06	84.5	93.4	1.25	−1.54	0.27

Note. $EM2_{major}$ and $EM3_{major}$ refer to the major populations of EM2 and EM3 (see Figures 5b and 5c). Mean, median and Std (standard deviation) were calculated after McManus (1988). CV: Coefficient of variation, CV = std/mean × 100%. Sorting, Skewness, and Kurtosis were calculated after (Folk & Ward, 1957).

period. EM2 and SC2 vary between 0 and 50.9% and between 9.57 and 32.6%, presenting higher and lower values at interglacial and glacial periods, respectively. EM3 and SC3 vary between 0 and 100% and between 11.6 and 32.0%, contrary to the distributions of EM2 and SC2, presenting higher and lower values at glacial and interglacial periods, respectively.

6. Discussion

6.1. Interpretations of Grain-Size End-Members

The P1–2 core site is located on the Prydz continental rise. Sediment supply to the study area mainly comes from the Antarctic continent. Pathways of nonbiogenic sediment supply to such deep sea setting include pelagic input from the sea surface (iceberg, sea ice, and dust), turbidites, and bottom currents (bottom nepheloid layers) (Gilbert et al., 1998; Pudsey, 1992).

Sea ice-related sediment transportation is limited here, because sea ice in the Prydz region forms over the deep continental shelf (several hundred meters), thus incorporating very little suspended sediments (e.g., Pudsey, 1992), unlike in the Arctic Ocean where dirty sea ice was commonly observed (Darby et al., 2009, 2011). Dust deposition can be neglected as well, because the region is far away from any dust source (Li et al., 2008). Turbidites and debris flows can also be ruled out, because sedimentary and bathymetric studies show that during the late Quaternary the LGAISS never grounded at the shelf break (Passchier et al., 2003), implying turbidity activity should be largely reduced as well. In addition, the P1–2 core site is located far from submarine canyons. The fine-grained nature and low sedimentation rate of the sediments and the

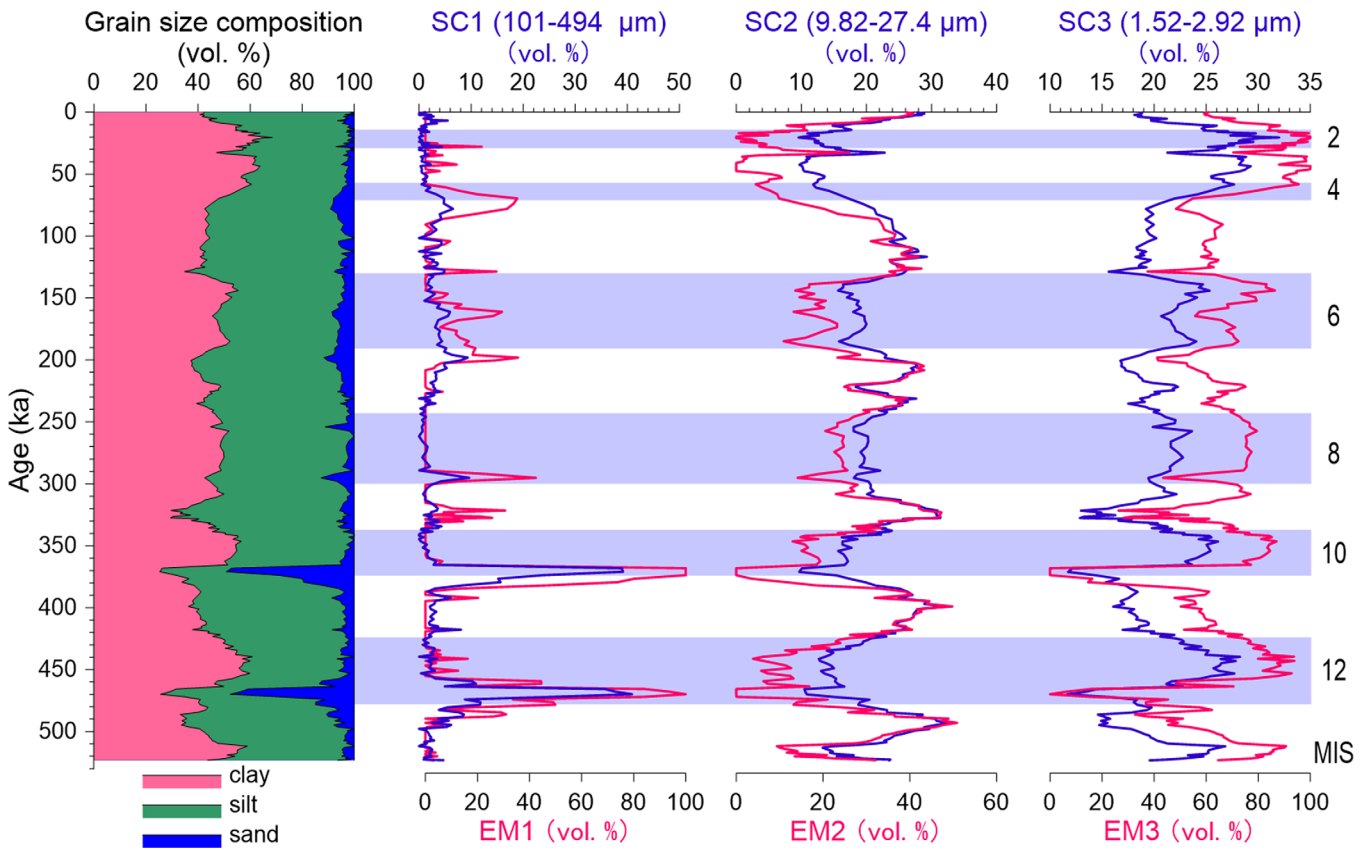

Figure 4. Temporal distributions of the EMMA-derived end-members and SGSM-derived sensitive grain size chasses. Also shown on the left is the grain size composition of the core sediments.

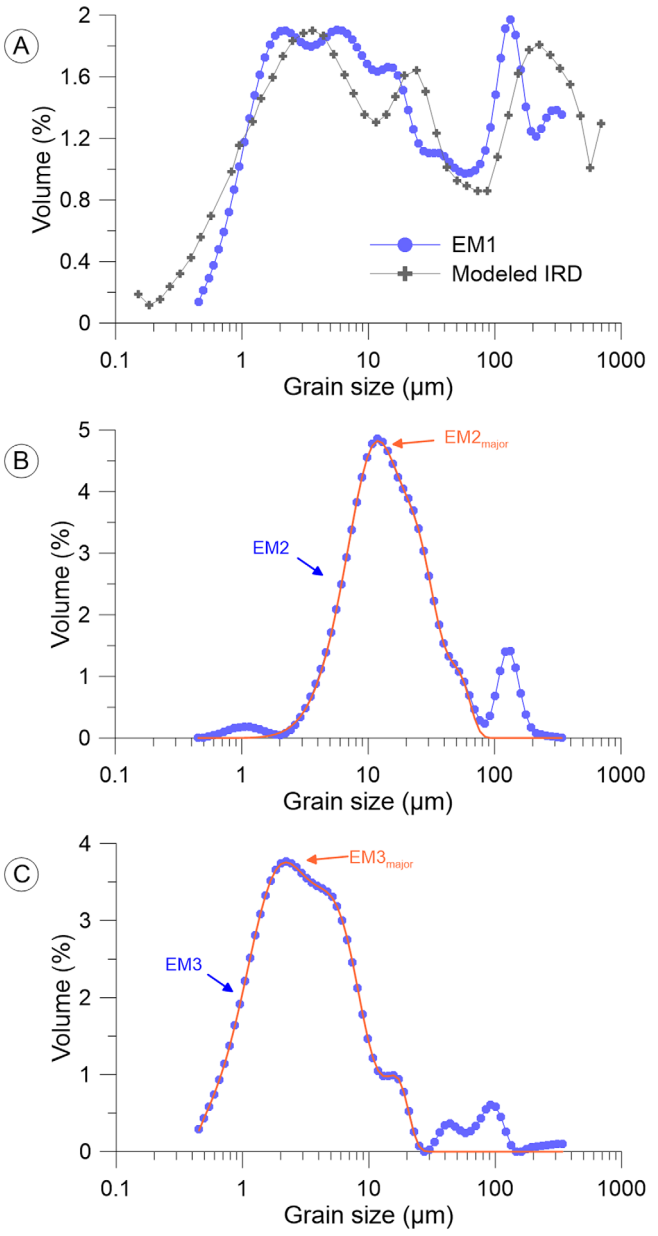

Figure 5. Grain-size distributions of (a) EM1 and modeled IRD from North Atlantic Ocean (Prins et al., 2002), (b) EM2 and its major population $EM2_{major}$, (c) EM3 and its major population $MEM3_{major}$.

absence of (turbidite-related) sedimentary structures all argue against a turbidite origin of the P1–2 core sediments.

EM1 (Figure 5A) is the coarsest end-member generated in this study with a mean grain size of 55.1 μm (Table 1). The grain-size distribution of EM1 is characterized by a poor sorting parameter (2.71) with grains of different diameters evenly distributed across the grain-size axis. The features of EM1 correspond well with the sediments carried by icebergs (Pudsey, 1992). EM1 is thus interpreted as the Ice Rafted Debris (IRD) end-member. The grain-size distribution pattern of EM1 is also largely consistent with that of previously modeled IRD end-members (e.g., Prins et al., 2002).

The temporal distributions of EM2 and EM3 show regular glacial-interglacial variabilities, with more EM2 (coarser EM) deposited during interglacials and more EM3 (finer EM) during glacial periods (Figure 4). EM2 and EM3 are polymodal (Figures 5b and 5c). But each of them has one major peak (at 12 and 2 μm, respectively). The major populations of EM2 ($EM2_{major}$) and EM3 ($EM3_{major}$) both account for $>$90 vol. % of the distributions of the two end-members (Figures 5b and 5c). Sorting parameters of the two major populations are 1.04 and 1.25, respectively (Table 1). Better sorting indicates that they may be selectively deposited from bottom nepheloid layers. Bottom nepheloid layers in deep sea basins are largely maintained by resuspension of bottom sediments (McCave, 1986), and the size distribution of sediments in suspension should relate closely to the strength of bottom currents (Pudsey, 1992). We thus interpret EM2 and EM3 representing coarse and fine sediments deposited from bottom nepheloid layers relating to strong and weak bottom current conditions, respectively. The secondary populations ($<$ 10 vol. %) in the two end-members (C5 in EM2 and C5 + C6 in EM3) are generally coarse-grained ($>$ 63 μm), overlapping with the coarse end of EM1. They likely reflect the random background IRD input, synchronously deposited with the bottom nepheloid layers.

With the knowledge of the three end-members, the three sensitive grain-size class (SC1–SC3) can be interpreted accordingly. SC1, SC2, and SC3 correspond to EM1, EM2, and EM3, representing IRD, coarse, and fine sediments deposited from bottom nepheloid layers, respectively.

6.2. Bottom Current Strength Inferred From Grain-Size Compositions

Conventionally, mean grain size of "sortable silt" fraction (10–63 μm) in deep sea sediments can be used to reveal bottom current strength (McCave et al., 1995; McCave & Hall, 2006). In polar oceans, the "sortable silt" fraction, however, is in many cases a mixture of material supplied by bottom currents and icebergs (e.g., Prins et al., 2002). In fact, the "sortable silt" proxy for bottom current strength was initially defined based on the "dynamical grain size" which is measured by Sedigraph or Coulter counter techniques (McCave et al., 1995; McCave & Hall, 2006). The two techniques measure the dynamical behavior of different sediment grains (McCave et al., 2006). Our grain-size data were measured using the "laser particle sizing" method, which measures the "morphological grain size" of sediments (the morphology of sediment grains) (McCave et al., 2006). Previous studies have shown that the "dynamical grain size" and the "morphological grain size" differ significantly, particularly when the sediments are fine-sized. The mean grain size of the "sortable silt" fraction calculated from laser particle sizing data therefore may produce misleading result (e.g., McCave et al., 2006). Thus, in this study we turn to infer the bottom current strength using the EMMA-derived end-members.

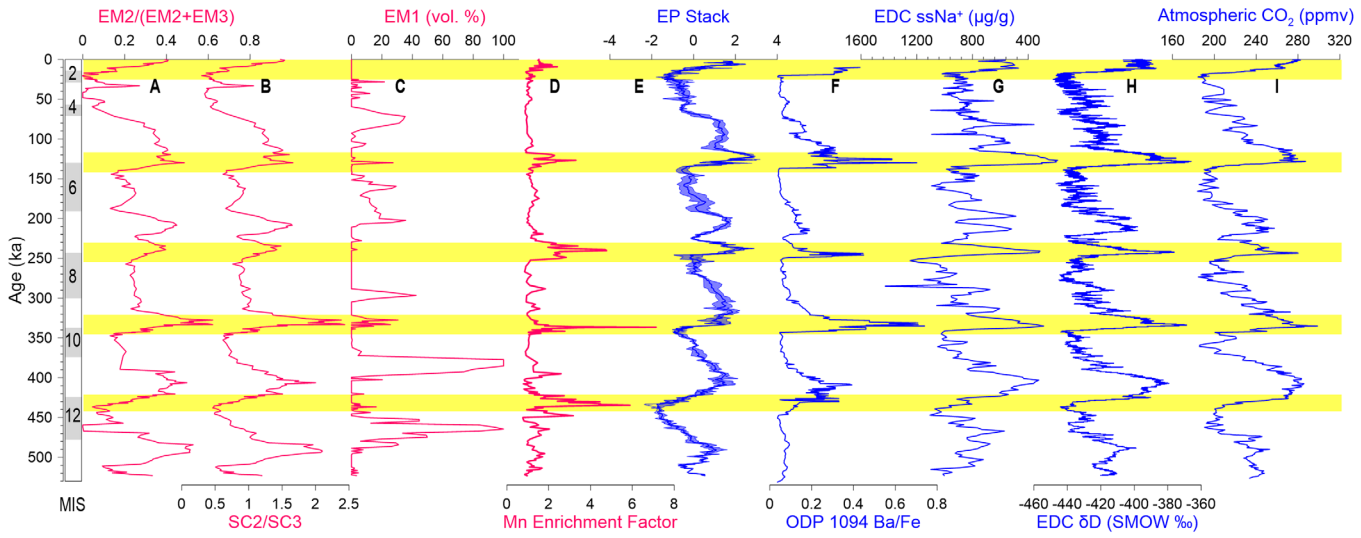

Figure 6. Temporal distributions of (a) EM2/(EM2 + EM3), (b) SC2/SC3, (c) EM1, (d) Mn enrichment factor, (e) EP Stack (Wu et al., 2017), (f) ODP 1094 Ba/Fe ratio (Jaccard et al., 2013), (g) EDC $ssNa^+$ (EPICA Community Members, 2004), (h) EDC δD (EPICA Community Members, 2004), and (i) Atmospheric CO_2 (EPICA Community Members, 2004). The light-blue shade behind the EP stack curve denotes the variation range of the normalized local export production.

Since EM2 and EM3 derived from EMMA, and SC2 and SC3 from sensitive grain size class model (SGSM) are interpreted as the coarse and fine materials deposited from bottom nepheloid layers, the ratios of EM2/(EM2 + EM3) and SC2/SC3 (Figures 6a and 6b) can be used as measures of the relative strength of the local bottom current without dilution from IRD input. The temporal distributions of EM2/(EM2 + EM3) and SC2/SC3 ratios present clear and coherent glacial-interglacial variations, indicating stronger and weaker bottom current strength during interglacial and glacial periods, respectively.

The variability of the bottom current strength may relate to a variety of mechanisms, such as, benthic storms (e.g., Spinrad & Zaneveld, 1982), internal tides, and waves (Dickson & McCave, 1986). However, neither of the above mechanisms can explain the glacial-interglacial change pattern of the deep current strength recorded in the sediments, as one cannot expect the benthic storms or internal tides and waves to be stronger during interglacial periods than during glacial periods. In fact, internal tides were possibly more vigorous in the glacial ocean because of the lower sea level (Egbert et al., 2004).

The P1–2 core site is located within the direct influence range of the ADZ—the southern boundary of the ACC, where the ASC and ACC actively interact with each other. The ASC and ACC are predominantly wind driven by the Southern Easterly Wind (SEW) and Southern Westerly Wind (SWW) stress, respectively. Mesoscale eddies extend the influence of the wind stress to the abyss, thereby affecting the abyssal circulations (Ito & Marshall, 2008; Johnson & Bryden, 1989; Toggweiler et al., 2006). Thus, changes in the wind speed and/or position directly influence the bottom current strength. On the other hand, variations in sea ice coverage at marginal seas around Antarctica also play an import role in modulating the abyssal current strength by changing the transmission of wind stress to the ocean (Lamy et al., 2015; McCave et al., 2014).

The northward expanding and intensification of SEW is always accompanied by synchronous expanding of sea ice coverage in wintertime, largely balancing the influence on the deep current speeds in the Southern Ocean (Mathiot et al., 2011). In contrast, the southward shift and intensification of SWW is accompanied by sea ice retreat in summer (Lamy et al., 2010), and could therefore play a more dynamical role changing the deep circulation under the ADZ and further north. This may hold during past glacial-interglacial variations as well, as stronger bottom current strength recorded in the grain-size data (Figures 6a and 6b) corresponds to strengthened/southward-shifted SWW and diminished sea ice cover (Figure 6g) during interglacial periods, while weaker bottom currents are synchronous with weakened/northward-shifted SWW and expanded sea ice (EPICA Community Members, 2004) during glacial periods (the shift pattern of the SWW cited here is the dominant view supported by most of the geological archives and some numerical simulations) (Kohfeld et al., 2013, and references therein). In fact, the grain size-inferred change pattern of the local deep

circulation here can be put into a more general deep circulation change mode in the Southern Ocean on glacial-interglacial timescale. Low-time resolution sediment records from the sea ice influenced Weddell Sea (Gilbert et al., 1998; Pudsey, 1992; Pudsey et al., 1988), Scotia sea (McCave et al., 2014), and the northern coast of the Drake Passage (Lamy et al., 2015) also indicate bottom current speeds decreased during glacial periods, simultaneous with the intensification of the deep western boundary current east of New Zealand, further demonstrating a combined effect of a northward shift of the SWW and ACC and enhanced sea ice cover in the Southern Ocean during glacial periods (Lamy et al., 2015; McCave et al., 2014; Pudsey, 1992).

Modern observations also indicate that the strength of the ASC can be intensified westward at places where AABW forms, e.g., near the Adelie Land region (Bindoff et al., 2000). This process, however, is very local. In the Prydz region, AABW forms off Cape Darney and flows westward along the slope due to the geostrophic force (Meijers et al., 2010), thus exerting limited influence on our core site.

6.3. AABW Formation Inferred From Mn Enrichments

Two different processes may cause the layered enrichments of Mn in the sediments during deglacial periods (Figure 6d): (1) transport and deposition of Mn-rich source materials (e.g., Jakobsson et al., 2000) and (2) an elevation in deep water oxygen concentration (e.g., Jaccard et al., 2016; Mangini et al., 2001; Presti et al., 2011).

Mn-rich sources may be the hydrothermal vents, lake systems, peat area, and well-vegetated area like bogs and forests (e.g., Jakobsson et al., 2000). The study area, however, is isolated from these sources. In addition, the Mn enrichment record (Figure 6d) is temporally inconsistent with the IRD record (EM1) (Figure 6c), indicating the excess Mn can neither be derived from old successions on land. Thus, we can only ascribe the Mn enrichments in the core sediments to elevated deep water oxygenation. Under oxygenated conditions, excess Mn supply can be caused by precipitation from overlying sea water and/or via upward diffusion from underlying successions (e.g., Jaccard et al., 2016; Mangini et al., 2001; Presti et al., 2011).

The fundamental control on redox states registered in abyssal sediments is the balance between the supply rate of oxygen from overlying bottom waters and the rate of pore-water oxygen removal associated primarily with organic carbon respiration (Jaccard et al., 2016). Since repletion in oxygen is one of the most prominent characteristics of newly formed AABW distinguishing from other abyssal water masses in the Southern Ocean, comparing the bottom water oxygen level by measuring sedimentary distributions of Mn with export production records thus provides an opportunity to qualitatively trace the variations in AABW formation and transportation.

Manganese concentrations are in general low in glacial sediments (Figure 6d). In combination with the low local export production (Figure 6e), which indicates low organic carbon exported to the abyssal ocean (Wu et al., 2017), this indicates a low AABW flux to the core site during glacial times. In contrast, during deglacial periods, the Southern Ocean deep water temperature was sharply elevated by $\sim$3°C (Elderfield et al., 2012) along with an increase in the Antarctic atmospheric temperature recorded in EDC-δD (Figure 6h), leading to a reduction in the ocean waters' solubility of O_2 by $>$20 μM (Galbraith & Jaccard, 2015; Jaccard & Galbraith, 2012). In combination with the enhanced local export production (Figure 6e), we conclude that the significant enrichment of Mn in the deglacial sediments is associated with abruptly improved oxygenation of the bottom water mass, signaling strengthened AABW formation and transportation to the core site. Our Mn enrichment factor record suggests the deglacial pulse of enhanced AABW formation is a common phenomenon in the Southern Ocean at every glacial termination of the Pleistocene.

The formation of AABW involves a series of shelf processes and deep water convection (Foster & Carmack, 1976; Orsi et al., 1999; Williams et al., 2008; Yabuki et al., 2006). It starts with the intrusion of the warm and salty CDW into the shelf and mixing of it with the cold, relatively fresh and oxygen-replete shelf waters. The mixed water mass then loses its buoyancy by densification via ice formation (either at the sea surface or under ice shelves) in winter. Then it overpasses sills on the shelf break and flows downward along slope valleys, where it mixes with the ambient water masses, ultimately forming AABW. Modern observations suggest sufficiently wide continental shelf space is an important environmental factor in favor of AABW formation (Fahrbach et al., 1994; Orsi et al., 1999), even at places where AABW formation is associated with polynia processes, e.g., the Adelie Land (Williams et al., 2008). This is because continental shelf space can help the precursor of AABW to remain saline (Yabuki et al., 2006), enabling it to sink to the basin floor.

Another factor affecting AABW formation is the CDW upwelling, which brings in salty CDW to the shelf regions, thereby promoting shelf mixing and densification processes (Foster & Carmack, 1976; Gill, 1973).

On the glacial-interglacial time scale, the retreat and advance of ice shelf groundling lines is the major factor controlling the available size of shelf space, while variations in the intensity of upper Southern Ocean upwelling, as indicated by the export production records south of APF (Figures 6e and 6f), limit the amount of CDW intruding into the shelf. The available continental shelf space and the intensity of Southern Ocean upwelling may therefore be the two major factors affecting the AABW formation rate over past glacial cycles.

6.4. Implication for Deep Stratification and Abyssal Carbon Storage

The grain size proxies for bottom current strength and the Mn enrichment series pertinent to the AABW formation constructed in this study show temporal distributions closely coupled with climate changes registered in other climate curves (Figure 6).

The bottom current strength, interacting with rough topography, influences the rate of deep water diapycnal mixing (mixing across isopycnal surfaces) in the Southern Ocean (Ito & Marshall, 2008; Marshall & Speer, 2012; McCave et al., 2014). Diapycnal mixing is an important mechanism leading to the lower and upper water masses to exchange with each other in the Southern Ocean (Wu et al., 2011). Stronger (weaker) bottom current strength would lead to higher (lower) diapycnal mixing rate and thus stronger (weaker) interaction between the lower and upper water masses (vice versa). AABW formation, on the other hand, directly links to Southern Ocean deep ventilation, representing another mechanism leading to the upper and lower water masses in the Southern Ocean to interact with each other (Jaccard et al., 2016). These processes may further profoundly affect Southern Ocean deep stratification and thereby the abyssal carbon storage (Ferrari et al., 2014; Marshall & Speer, 2012; Watson & Naveira Garabato, 2006).

There is a consensus that during LGM, waters of North Atlantic origin only sank to a shallower depth, forming the Glacial North Atlantic Intermediate Water (GNAIW), with the remaining ocean basins (except for the Arctic Ocean) being mainly filled with waters of Antarctic origin (Ferrari et al., 2014; Lippold et al., 2016; Sikes et al., 2016), although the strength of MOC might be similar with that of present days' (Lippold et al., 2012; Ritz et al., 2013). The glacial upper Southern Ocean was much more stratified than today based on measurements of the diatom-bound nitrogen isotope compositions (Horn et al., 2011; Robinson & Sigman, 2008; Studer et al., 2015). A northward shift/weakening of SWW, in combination with a northward expansion of sea ice cover largely prevented wind-related momentum from transmitting into the ocean, and consequently reduced the wind-driven, eddy-induced CDW upwelling (Anderson et al., 2009, 2014; Jaccard et al., 2013) as well as the bottom current speeds (Figures 6a and 6b). The reduced upwelling may further diminish CDW from intruding into the shelf, in combination with a narrowing of the shelf space due to advancing of continental ice grounding lines (Pollard & DeConto, 2009). Waters of Antarctic origin might only sink into shallower depths because of efficient buoyancy gain from mixing with ambient waters, given a lack of shelf spaces to keep their salinity (Yabuki et al., 2006), resulting in a reduction in AABW formation. Meanwhile, the reduced bottom current speeds imply diapycnal mixing in deep Southern Ocean was reduced as well (McCave et al., 2014). Reductions in AABW formation and deep diapycnal mixing thus synergically suggest an enhancement in the deep stratification (Ferrari et al., 2014), which allowed more time for respired organic carbon to accumulate in the deep Southern Ocean (Jaccard et al., 2016; Wagner & Hendy, 2017; Watson & Naveira Garabato, 2006), as shown in Figure7a. The accumulation of CO_2 further increased the alkalinity of deep water masses, promoting the solubility of CO_2 in deep Southern Ocean (Keir, 1988), and finally contributing to glacial atmospheric CO_2 drawdown (Figure 6i).

During deglacial periods (Figure 7b), the ocean circulation pattern experienced dramatic changes. The volume of abyssal waters of Antarctic origin contracted, and became largely replaced by reinvigorated, well-ventilated North Atlantic Deep Water (NADW) (Ferrari et al., 2014; Lippold et al., 2016; Sikes et al., 2016). The southward shift/intensification of SWW (Kohfeld et al., 2013) and the retreat of sea ice coverage enhanced Southern Ocean upwelling (Anderson et al., 2009; Jaccard et al., 2013; Wu et al., 2017) as well as the deep circulation (Figures 6a and 6b). The enhanced upwelling promoted intrusion of CDW into the shelf, in combination with the elevated atmospheric temperature (Figure 6h) (EPICA Community Members, 2004), leading into the melting of land ice and consequent retreat of ice grounding lines (Pollard & DeConto, 2009), thereby favoring dense waters, produced by brine rejection when sea ice forms, to sink to the abyss to form

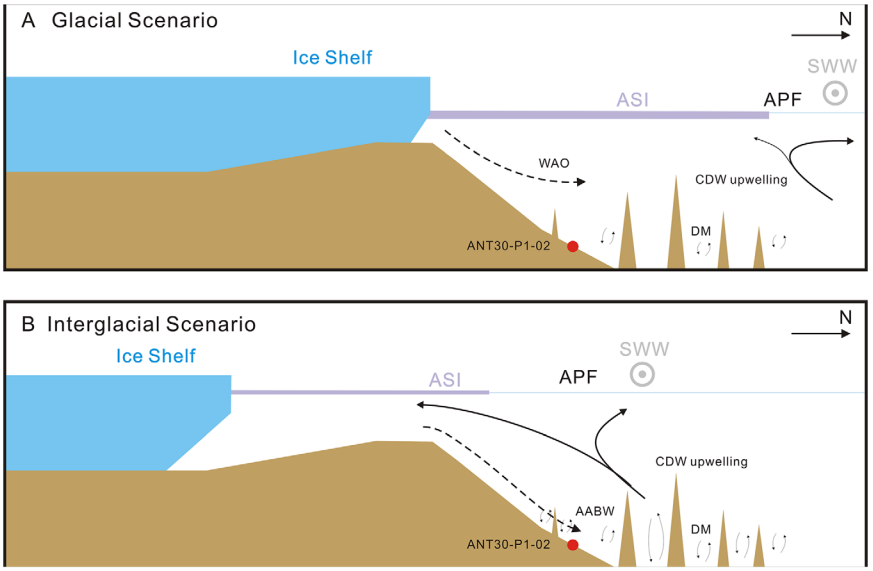

Figure 7. Schematic diagram for glacial-interglacial changes in the vertical Southern Ocean structure. (a) The Glacial (maximum) scenario. (b) The glacial termination scenario. ASI: average sea ice coverage; APF: Antarctic Polar Front; SWW: Southern Westerly Wind; WAO: waters of Antarctic origin; AABW: Antarctic bottom water; CDW: Circumpolar Deep Water; DM: diapycnal mixing.

AABW. The elevated AABW formation and enhanced deep circulation alleviated previously enhanced deep stratification by efficiently interacting with the upper Southern Ocean via diapycnal mixing at rough topographies (Ferrari et al., 2014; McCave et al., 2014), leading to deeply sequestered CO_2 to diffuse upward and ultimately outgas with the upper Southern Ocean upwelling (Figure 6i) (Anderson et al., 2009; Jaccard et al., 2016; Marshall & Speer, 2012).

After peak interglacial conditions, with climate cooling, SWW shifted northward/weakened, and sea ice expanded again (Bazin et al., 2013; EPICA Community Members, 2004). The upper Southern Ocean became more and more stratified (Jaccard et al., 2013; Wu et al., 2017), weakening CDW upwelling (Figures 6e and 6f), and the deep circulation (Figures 6a and 6b). We conclude that the deep Southern Ocean possibly became increasingly stratified as well. Deeply sequestered CO_2 was thus more and more difficult to escape from the abyss, in combination with the effect of the "biological pump" (Galbraith & Jaccard, 2015; Jaccard et al., 2013, 2016), leading to gradual drawdown of the atmospheric CO_2 and its build-up in the abyss (Figure 6i).

Our data thus may suggest that the interior of the deep Southern Ocean also underwent synchronous changes with changes in the upper Southern Ocean. The sea ice and SWW configurations may be the major driving force of the physical changes in the deep Southern Ocean (Ferrari et al., 2014; Lamy et al., 2015; McCave et al., 2014). The abyssal carbon storage, however, may be affected by a series processes involving the atmosphere, ocean as well as the cryosphere.

7. Conclusions

In this study, we report the grain-size distributions as well as the Mn geochemistry of a sediment core ANT30/P1-02 retrieved off Prydz Bay, East Antarctica. Major conclusions are drawn as follows:

1. The late Quaternary core sediments are predominantly composed of clay and silt-sized materials with minor sand fraction, except for two layers at the lower section. Three end-members as well as three corresponding sensitive grain size classes were extracted from the grain-size distributions of the core sediments using an End-Member Modeling Algorithm (EMMA) and a Sensitive Grain Size Class Model. EM1 and SC1 are interpreted as IRD. EM2 and SC2, and EM3 and SC3 are interpreted as coarse and fine materials deposited from bottom nepheloid layers, respectively.
2. The ratios of EM2/(EM2 + EM3) and SC2/SC3 reflect changes in the local bottom current strength. They generally show higher values during interglacial periods and lower values during glacial periods,

indicating stronger and weaker bottom current strength during interglacial and glacial periods, respectively. The changes in the bottom current strength were mainly controlled by SWW intensity/position and modulated by sea ice cover, revealing the changes in the rate of deep Southern Ocean diapycnal mixing.

3. Mn enrichment factor varies between 0.762 and 7.134, predominantly showing higher values at every glacial termination of the past 523 kyrs. The glacial-interglacial variation in AABW flux to the study area is inferred by comparing the Mn enrichment factor with the local export production record. Such comparison indicates abrupt elevations in AABW fluxes to the study area during glacial terminations. We suggest the available continental shelf space controlled by position of ice shelf grounding lines and the intensity of Southern Ocean upwelling are the two major environmental factors affecting past AABW formation.
4. Variations in AABW formation and deep current strength reveal the deep ventilation and circulation history of the Southern Ocean. Reductions in AABW formation and deep current strength during glacial periods, due to the northward shift/weakening of SWW and expanded sea ice cover, enhanced the deep Southern Ocean stratification, thereby allowing more time for respired organic carbon to build-up, contributing to glacial atmospheric CO_2 drawdown. During deglacial periods, the elevated AABW formation and enhanced deep circulation as a result of southward shift/intensification of SWW and retreat of sea ice alleviated the deep stratification, leading to deeply sequestered CO_2 to diffuse upward and ultimately outgas through the upper Southern Ocean upwelling. After peak interglacial conditions, the deep Southern Ocean became more and more stratified again.

Acknowledgments
We are most grateful to the two anonymous reviewers for their constructive comments that helped to improve greatly the manuscript. This work is financially supported by the National Natural Science Foundation of China (grant 41776191). It is also part of the project "the 30th Chinese National Antarctic Research Expedition" (CHINARE-2013) organized by the Chinese Arctic and Antarctic Administration (CAA) and supported by Ministry of Finance of China (CHINARE-2012-2020-01-02). We thank the 30th Chinese Antarctic Expedition cruise members for retrieving the sediments. The data sets analyzed during the current study can be downloaded as the supporting information and will also be made available at www.pangaea.de

References

Abe-Ouchi, A., Saito, F., Kawamura, K., Raymo, M. E., Okuno, J. I., Takahashi, K., & Blatter, H. (2013). Insolation-driven 100,000-year glacial cycles and hysteresis of ice-sheet volume. *Nature*, *500*(7461), 190–193. https://doi.org/10.1038/nature12374

Abelmann, A., Gersonde, R., Cortese, G., Kuhn, G., & Smetacek, V. (2006). Extensive phytoplankton blooms in the Atlantic sector of the glacial Southern Ocean. *Paleoceanography*, *21*, PA1013. https://doi.org/10.1029/2005PA001199

Abelmann, A., Gersonde, R., Knorr, G., Zhang, X., Chapligin, B., Maier, E., et al. (2015). The seasonal sea-ice zone in the glacial Southern Ocean as a carbon sink. *Nature Communications*, *6*, 8136. https://doi.org/10.1038/ncomms9136

Adkins, J. F., McIntyre, K., & Schrag, D. P. (2002). The salinity, temperature, and delta O-18 of the glacial deep ocean. *Science*, *298*(5599), 1769–1773. https://doi.org/10.1126/science.1076252

Anderson, R. F., Ali, S., Bradtmiller, L. I., Nielsen, S. H. H., Fleisher, M. Q., Anderson, B. E., & Burckle, L. H. (2009). Wind-driven upwelling in the Southern Ocean and the deglacial rise in atmospheric CO_2. *Science*, *323*(5920), 1443–1448. https://doi.org/10.1126/science.1167441

Anderson, R. F., Barker, S., Fleisher, M., Gersonde, R., Goldstein, S. L., Kuhn, G., . . . Sachs, J. P. (2014). Biological response to millennial variability of dust and nutrient supply in the subAntarctic South Atlantic Ocean. *Royal Society of London Philosophical Transactions Series A*, *372*(2019), 20130054. https://doi.org/10.1098/rsta.2013.0054

Bazin, L., Landais, A., Lemieux-Dudon, B., Toyé Mahamadou Kele, H., Veres, D., Parrenin, F.et al. (2013). An optimized multi-proxy, multi-site Antarctic ice and gas orbital chronology (AICC2012): 120–800 ka. *Climate of the Past*, *9*(4), 1715–1731. https://doi.org/10.5194/cp-9-1715-2013

Bindoff, N. L., Rosenberg, M. A., & Warner, M. J. (2000). On the circulation and water masses over the Antarctic continental slope and rise between 80 and 150°E. *Deep Sea Research Part II: Topical Studies in Oceanography*, *47*(12–13), 2299–2326. https://doi.org/10.1016/S0967-0645(00)00038-2

Boulay, S., Colin, C., Trentesaux, A., Pluquet, F., Bertaux, J., Blamart, D., et al. (2003). Mineralogy and sedimentology of Pleistocene sediment in the South China Sea (ODP Site 1144). In W. L. Prell et al. (Eds.), *Proceedings of the Ocean Drilling Program Scientific Results* (Vol. 184, pp. 1–21). College Station, TX: Ocean Drilling Program.

Brovkin, V., Ganopolski, A., Archer, D., & Rahmstorf, S. (2007). Lowering of glacial atmospheric CO_2 in response to changes in oceanic circulation and marine biogeochemistry. *Paleoceanography*, *22*, PA4202. https://doi.org/10.1029/2006PA001380

Burke, A., & Robinson, L. F. (2012). The Southern Ocean's role in carbon exchange during the last deglaciation. *Science*, *335*(6068), 557–561. https://doi.org/10.1126/science.1208163

Cooper, A. K., & O'Brien, P. E. (2004). Leg 188 synthesis: Transitions in the glacial history of the Prydz Bay region, East Antarctica, from ODP drilling. *Proceedings of the Ocean Drilling Program Scientific Results*, *188*, 1–42.

Crosta, X., Pichon, J. J., & Burckle, L. (1998a). Application of modern analog technique to marine Antarctic diatoms: Reconstruction of maximum sea ice extent at the Last Glacial Maximum. *Paleoceanography*, *13*(3), 284–297. https://doi.org/10.1029/98PA00339

Crosta, X., Pichon, J. J., & Burckle, L. H. (1998b). Reappraisal of Antarctic seasonal sea ice at the Last Glacial Maximum. *Geophysical Research Letters*, *25*(14), 2703–2706. https://doi.org/10.1029/98GL02012

Darby, D. A., Myers, W. B., Jakobsson, M., & Rigor, I. (2011). Modern dirty sea ice characteristics and sources: The role of anchor ice. *Journal of Geophysical Research*, *116*, C09008. https://doi.org/10.1029/2010JC006675

Darby, D. A., Ortiz, J., Polyak, L., Lund, S., Jakobsson, M., & Woodgate, R. (2009). The role of currents and sea ice in both slowly deposited central Arctic and rapidly deposited Chukchi–Alaskan margin sediments. *Global and Planetary Change*, *68*(1–2), 58–72. https://doi.org/10.1016/j.gloplacha.2009.02.007

Dickson, R. R., & McCave, I. N. (1986). Nepheloid layers on the continental-slope west of Forcupine Bank. *Deep Sea Research Part A: Oceanographic Research Papers*, *33*(6), 791–818. https://doi.org/10.1016/0198-0149(86)90089-0

Egbert, G. D., Ray, R. D., & Bills, B. G. (2004). Numerical modeling of the global semidiurnal tide in the present day and in the last glacial maximum. *Journal of Geophysical Research*, *109*, C03003. https://doi.org/10.1029/2003JC001973

Elderfield, H., Ferretti, P., Greaves, M., Crowhurst, S., McCave, I. N., Hodell, D., & Piotrowski, A. M. (2012). Evolution of ocean temperature and ice volume through the mid-Pleistocene climate transition. *Science*, *337*, 704–710. https://doi.org/10.1126/science.1221294

Elderfield, H., & Rickaby, R. E. M. (2000). Oceanic Cd/P ratio and nutrient utilization in the glacial Southern Ocean. *Nature*, *405*(6784), 305–310. https://doi.org/10.1038/35012507

EPICA Community Members. (2004). Eight glacial cycles from an Antarctic ice core. *Nature*, *429*, 623–628. https://doi.org/10.1038/nature02599

Fahrbach, E., Peterson, R. G., Rohardt, G., Schlosser, P., & Bayer, R. (1994). Suppression of bottom water formation in the southeastern Weddell sea. *Deep Sea Research Part I: Oceanographic Research Papers*, *41*(2), 389–411. https://doi.org/10.1016/0967-0637(94)90010-8

Ferrari, R., Jansen, M. F., Adkins, J. F., Burke, A., Stewart, A. L., & Thompson, A. F. (2014). Antarctic sea ice control on ocean circulation in present and glacial climates. *Proceedings of the National Academy of Sciences of the United States of America*, *111*(24), 8753–8758. https://doi.org/10.1073/pnas.1323922111

Foldvik, A., Gammelsrød, T., Østerhus, S., Fahrbach, E., Rohardt, G., Schröder, M., et al. (2004). Ice shelf water overflow and bottom water formation in the southern Weddell Sea. *Journal of Geophysical Research*, *109*, C02015. https://doi.org/10.1029/2003JC002008

Folk, R. L., & Ward, W. C. (1957). Brazos River bar: A study in the significance of grain size parameters. *Journal of Sedimentary Research*, *27*(1), 3–26. https://doi.org/10.1306/74D70646-2B21-11D7-8648000102C1865D

Forsberg, C. F., Florindo, F., Grützner, J., Venuti, A., & Solheim, A. (2008). Sedimentation and aspects of glacial dynamics from physical properties, mineralogy and magnetic properties at ODP Sites 1166 and 1167, Prydz Bay, Antarctica. *Palaeogeography, Palaeoclimatology, Palaeoecology*, *260*(1–2), 184–201. https://doi.org/10.1016/j.palaeo.2007.08.022

Foster, T. D., & Carmack, E. C. (1976). Frontal zone mixing and Antarctic Bottom water formation in the southern Weddell Sea. *Deep Sea Research and Oceanographic Abstracts*, *23*(4), 301–317. https://doi.org/10.1016/0011-7471(76)90872-X

Frank, M., Gersonde, R., van der Loeff, M. R., Bohrmann, G., Nürnberg, C. C., Kubik, P. W., et al. (2000). Similar glacial and interglacial export bioproductivity in the Atlantic sector of the Southern Ocean: Multiproxy evidence and implications for glacial atmospheric CO_2. *Paleoceanography*, *15*(6), 642–658. https://doi.org/10.1029/2000PA000497

Galbraith, E. D., & Jaccard, S. L. (2015). Deglacial weakening of the oceanic soft tissue pump: Global constraints from sedimentary nitrogen isotopes and oxygenation proxies. *Quaternary Science Reviews*, *109*, 38–48. https://doi.org/10.1016/j.quascirev.2014.11.012

Garcia, H. E., Locarnini, R. A., & Boyer, T. P. (2009). Dissolved oxygen, apparent oxygen utilization, and oxygen saturation. In *World Ocean Atlas 3*. Washington, DC: Government Printing Office.

Gersonde, R., Crosta, X., Abelmann, A., & Armand, L. (2005). Sea-surface temperature and sea ice distribution of the Southern Ocean at the EPILOG Last Glacial Maximum: A circum-Antarctic view based on siliceous microfossil records. *Quaternary Science Reviews*, *24*(7–9), 869–896. https://doi.org/10.1016/j.quascirev.2004.07.015

Gilbert, I. M., Pudsey, C. J., & Murray, J. W. (1998). A sediment record of cyclic bottom-current variability from the northwest Weddell Sea. *Sedimentary Geology*, *115*(1–4), 185–214. https://doi.org/10.1016/S0037-0738(97)00093-6

Gill, A. E. (1973). Circulation and bottom water production in the Weddell Sea. *Deep Sea Research and Oceanographic Abstracts*, *20*(2), 111–140. https://doi.org/10.1016/0011-7471(73)90048-X

Goosse, H., Roche, D., Mairesse, A., & Berger, M. (2013). Modelling past sea ice changes. *Quaternary Science Reviews*, *79*, 191–206. https://doi.org/10.1016/j.quascirev.2013.03.011

Hain, M. P., Sigman, D. M., & Haug, G. H. (2010). Carbon dioxide effects of Antarctic stratification, North Atlantic Intermediate Water formation, and subAntarctic nutrient drawdown during the last ice age: Diagnosis and synthesis in a geochemical box model. *Global Biogeochemical Cycles*, *24*, GB4023. https://doi.org/10.1016/j.quaint.2012.08.294

Hannah, M. J. (2006). The palynology of ODP site 1165, Prydz Bay, East Antarctica: A record of Miocene glacial advance and retreat. *Palaeogeography, Palaeoclimatology, Palaeoecology*, *231*(1–2), 120–133. https://doi.org/10.1016/j.palaeo.2005.07.029

Horn, M. G., Beucher, C. P., Robinson, R. S., & Brzezinski, M. A. (2011). Southern ocean nitrogen and silicon dynamics during the last deglaciation. *Earth and Planetary Science Letters*, *310*(3–4), 334–339. https://doi.org/10.1016/j.epsl.2011.08.016

Ito, T., & Marshall, J. (2008). Control of lower-limb overturning circulation in the Southern Ocean by diapycnal mixing and mesoscale eddy transfer. *Journal of Physical Oceanography*, *38*(12), 2832–2845. https://doi.org/10.1175/2008JPO3878.1

Jaccard, S. L., & Galbraith, E. D. (2012). Large climate-driven changes of oceanic oxygen concentrations during the last deglaciation. *Nature Geoscience*, *5*(2), 151–156. https://doi.org/10.1038/ngeo1352

Jaccard, S. L., Galbraith, E. D., Martínez-García, A., & Anderson, R. F. (2016). Covariation of deep Southern Ocean oxygenation and atmospheric CO_2 through the last ice age. *Nature*, *530*(7589), 207–210. https://doi.org/10.1038/nature16514

Jaccard, S. L., Hayes, C. T., Martínez-García, A., Hodell, D., Anderson, R. F., Sigman, D., & Haug, G. (2013). Two modes of change in Southern Ocean productivity over the past million years. *Science*, *339*(6126), 1419–1423. https://doi.org/10.1126/science.1227545

Jakobsson, M., Løvlie, R., Al-Hanbali, H., Arnold, E., Backman, J., & Mörth, M. (2000). Manganese and color cycles in Arctic Ocean sediments constrain Pleistocene chronology. *Geology*, *28*, 23–26. https://doi.org/10.1130/0091-7613(2000)28<23:MACCIA>2.0.CO;2

Johnson, G. C., & Bryden, H. L. (1989). On the size of the Antarctic circumpolar current. *Deep-Sea Research Part A: Oceanographic Research Papers*, *36*(1), 39–53. https://doi.org/10.1016/0198-0149(89)90017-4

Jonkers, L., Barker, S., Hall, I., & Prins, M. (2015). Correcting for the influence of ice-rafted detritus on grain size-based paleocurrent speed estimates. *Paleoceanography and Paleoclimatology*, *30*(10), 1347–1357. https://doi.org/10.1002/2015PA002830

Jonkers, L., Prins, M. A., Brummer, G. J. A., Konert, M., & Lougheed, B. C. (2009). Experimental insights into laser diffraction particle sizing of fine-grained sediments for use in palaeoceanography. *Sedimentology*, *56*(7), 2192–2206. https://doi.org/10.1111/j.1365-3091.2009.01076.x

Keir, R. S. (1988). On the late Pleistocene ocean geochemistry and circulation. *Paleoceanography*, *3*(4), 413–445. https://doi.org/10.1029/PA003i004p00413

Knox, F., & McElroy, M. B. (1984). Changes in atmospheric CO_2-influence of the marine biota at high-latitude. *Journal of Geophysical Research*, *89*(D3), 4629–4637. https://doi.org/10.1029/JD089iD03p04629

Kohfeld, K. E., Graham, R. M., de Boer, A. M., Sime, L. C., Wolff, E. W., Le Quéré, C., & Bopp, L. (2013). Southern Hemisphere westerly wind changes during the Last Glacial Maximum: Paleo-data synthesis. *Quaternary Science Reviews*, *68*, 76–95. https://doi.org/10.1016/j.quascirev.2013.01.017

Kumar, N., Anderson, R., Mortlock, R., Froelich, P., Kubik, P., Dittrich-Hannen, B., & Suter, M. (1995). Increased biological productivity and export production in the glacial Southern Ocean. *Nature*, *378*(6558), 675–680. https://doi.org/10.1038/378675a0

Lamy, F., Arz, H. W., Kilian, R., Lange, C. B., Lembke-Jene, L., Wengler, M., et al. (2015). Glacial reduction and millennial-scale variations in Drake Passage throughflow. *Proceedings of the National Academy of Sciences of the United States of America*, *112*(44), 13496–13501. https://doi.org/10.1073/pnas.1509203112

Lamy, F., Kilian, R., Arz, H. W., Francois, J.-P., Kaiser, J., Prange, M., & Steinke, T. (2010). Holocene changes in the position and intensity of the southern westerly wind belt. *Nature Geoscience*, *3*(10), 695–699. https://doi.org/10.1038/NGEO959

Li, F., Ginoux, P., & Ramaswamy, V. (2008). Distribution, transport, and deposition of mineral dust in the Southern Ocean and Antarctica: Contribution of major sources. *Journal of Geophysical Research*, *113*, D10207. https://doi.org/10.1029/2007JD009190

Lippold, J., Gutjahr, M., Blaser, P., Christner, E., de Carvalho Ferreira, M. L., Mulitza, S., et al. (2016). Deep water provenance and dynamics of the (de)glacial Atlantic meridional overturning circulation. *Earth and Planetary Science Letters*, *445*, 68–78. https://doi.org/10.1016/j.epsl.2016.04.013

Lippold, J., Luo, Y., Francois, R., Allen, S. E., Gherardi, J., Pichat, S., et al. (2012). Strength and geometry of the glacial Atlantic Meridional Overturning Circulation. *Nature Geoscience*, *5*(11), 813–816. https://doi.org/10.1038/NGEO1608

Lisiecki, L. E., & Raymo, M. E. (2005). A Pliocene-Pleistocene stack of 57 globally distributed benthic δ18O records. *Paleoceanography*, *20*, PA1003. https://doi.org/10.1029/2005PA001164

Mangini, A., Jung, M., & Laukenmann, S. (2001). What do we learn from peaks of uranium and of manganese in deep sea sediments?. *Marine Geology*, *177*(1–2), 63–78. https://doi.org/0.1016/S0025-3227(01)00124-4

Marshall, J., & Speer, K. (2012). Closure of the meridional overturning circulation through Southern Ocean upwelling. *Nature Geoscience*, *5*(3), 171–180. https://doi.org/10.1038/NGEO1391

Martínez-García, A., Sigman, D. M., Ren, H., Anderson, R. F., Straub, M., Hodell, D. A., et al. (2014). Iron fertilization of the subAntarctic Ocean during the last ice age. *Science*, *343*(6177), 1347–1350. https://doi.org/10.1126/science.1246848

Mathiot, P., Goosse, H., Fichefet, T., Barnier, B., & Gallée, H. (2011). Modelling the seasonal variability of the Antarctic Slope current. *Ocean Science*, *7*(4), 455–532. https://doi.org/10.5194/os-7-455-2011

McCave, I. N. (1986). Local and global aspects of the bottom nepheloid layers in the world ocean. *Netherlands Journal of Sea Research*, *20*(2–3), 167–181.

McCave, I. N., Crowhurst, S. J., Kuhn, G., Hillenbrand, C. D., & Meredith, M. P. (2014). Minimal change in Antarctic Circumpolar Current flow speed between the last glacial and Holocene. *Nature Geoscience*, *7*(2), 113–116. https://doi.org/10.1038/NGEO2037

McCave, I. N., & Hall, I. R. (2006). Size sorting in marine muds: Processes, pitfalls, and prospects for paleoflow-speed proxies. *Geochemistry, Geophysics, Geosystems*, *7*, Q10N05. https://doi.org/10.1029/2006GC001284

McCave, I. N., Hall, I. R., & Bianchi, G. G. (2006). Laser vs. settling velocity differences in silt grain-size measurements: Estimation of palaeocurrent vigour. *Sedimentology*, *53*(4), 919–928. https://doi.org/10.1111/j.1365-3091.2006.00783.x

McCave, I. N., Manighetti, B., & Robinson, S. G. (1995). Sortable silt and fine sediment size composition slicing-parameters for paleocurrent speed and *Paleoceanography*. *Paleoceanography*, *10*(3), 593–610. https://doi.org/10.1029/94PA03039

Meijers, A. J. S., Klocker, A., Bindoff, N. L., Williams, G. D., & Marsland, S. J. (2010). The circulation and water masses of the Antarctic shelf and continental slope between 30 and 80°E. *Deep Sea Research Part II: Topical Studies in Oceanography*, *57*(9–10), 723–737. https://doi.org/10.1016/j.dsr2.2009.04.019

Moore, J. K., Abbott, M. R., Richman, J. G., & Nelson, D. M. (2000). The Southern Ocean at the last glacial maximum: A strong sink for atmospheric carbon dioxide. *Global Biogeochemical Cycles*, *14*(1), 455–475.

Nolting, R., Ramkema, A., & Everaarts, J. (1999). The geochemistry of Cu, Cd, Zn, Ni and Pb in sediment cores from the continental slope of the Banc d'Arguin (Mauritania). *Continental Shelf Research*, *19*(5), 665–691.

Nunes Vaz, R. A., & Lennon, G. W. (1996). Physical oceanography of the Prydz Bay region of Antarctic waters. *Deep Sea Research Part I: Oceanographic Research Papers*, *43*(5), 603–641.

Ohshima, K. I., Fukamachi, Y., Williams, G. D., Nihashi, S., Roquet, F., Kitade, Y., et al. (2013). Antarctic Bottom Water production by intense sea-ice formation in the Cape Darnley polynya. *Nature Geoscience*, *6*(3), 235–240. https://doi.org/10.1038/ngeo1738

Orsi, A. H., Johnson, G. C., & Bullister, J. L. (1999). Circulation, mixing, and production of Antarctic Bottom Water. *Progress in Oceanography*, *43*(1), 55–109.

Passchier, S., O'brien, P., Damuth, J., Januszczak, N., Handwerger, D., & Whitehead, J. (2003). Pliocene–Pleistocene glaciomarine sedimentation in eastern Prydz Bay and development of the Prydz trough-mouth fan, ODP Sites 1166 and 1167, East Antarctica. *Marine Geology*, *199*(3–4), 279–305.

Pollard, D., & DeConto, R. M. (2009). Modelling West Antarctic ice sheet growth and collapse through the past five million years. *Nature*, *458*(7236), 329–332. https://doi.org/10.1038/nature07809

Presti, M., Barbara, L., Denis, D., Schmidt, S., De Santis, L., & Crosta, X. (2011). Sediment delivery and depositional patterns off Adélie Land (East Antarctica) in relation to late Quaternary climatic cycles. *Marine Geology*, *284*(1–4), 96–113. https://doi.org/10.1016/j.margeo.2011.03.012

Prins, M. A., Bouwer, L. M., Beets, C. J., Troelstra, S. R., Weltje, G. J., Kruk, R. W., et al. (2002). Ocean circulation and iceberg discharge in the glacial North Atlantic: Inferences from unmixing of sediment size distributions. *Geology*, *30*(6), 555–558.

Prins, M. A., Postma, G., & Weltje, G. (2000). Controls on terrigenous sediment supply to the Arabian Sea during the late Quaternary: The Makran continental slope. *Marine Geology*, *169*(3–4), 351–371.

Prins, M. A., & Weltje, G. (1999). End-member modeling of siliciclastic grain-size distributions: The late Quaternary record of aeolian and fluvial sediment supply to the Arabian Sea and its paleoclimatic significance. In J. Harbaugh (Ed.), *Numerical experiments in stratigraphy: Recent advances in stratigraphic and sedimentologic computer simulations*, SEPM Special Publication (Vol. 62, pp. 91–111). Tulsa, OK: Society for Sedimentary Geology.

Pudsey, C. J. (1992). Late quaternary changes in Antarctic bottom water velocity inferred from sediment grain size in the northern Weddell Sea. *Marine Geology*, *107*(1–2), 9–33.

Pudsey, C. J., Barker, P. F., & Hamilton, N. (1988). Weddell Sea abyssal sediments a record of Antarctic bottom water flow. *Marine Geology*, *81*(1–4), 289–314.

Ritz, S. P., Stocker, T. F., Grimalt, J. O., Menviel, L., & Timmermann, A. (2013). Estimated strength of the Atlantic overturning circulation during the last deglaciation. *Nature Geoscience*, *6*(3), 208–212. https://doi.org/10.1038/ngeo1723

Roberson, S., & Weltje, G. J. (2014). Inter-instrument comparison of particle-size analysers. *Sedimentology*, *61*(4), 1157–1174. https://doi.org/10.1111/sed.12093

Robinson, R. S., & Sigman, D. M. (2008). Nitrogen isotopic evidence for a poleward decrease in surface nitrate within the ice age Antarctic. *Quaternary Science Reviews*, *27*(9–10), 1076–1090. https://doi.org/10.1016/j.quascirev.2008.02.005

Röthlisberger, R., Crosta, X., Abram, N. J., Armand, L., & Wolff, E. W. (2010). Potential and limitations of marine and ice core sea ice proxies: An example from the Indian Ocean sector. *Quaternary Science Reviews*, *29*, 296–302. https://doi.org/10.1016/j.quascirev.2008.02.005

Sarmiento, J. L., & Toggweiler, J. R. (1984). A new model for the role of the oceans in determining atmospheric PCO_2. *Nature*, *308*(5960), 621–624.

Schlitzer, R. (2009). *Ocean Data View Software*. Retrieved from http://odv.awi.de/

Schmitt, J., Schneider, R., Elsig, J., Leuenberger, D., Lourantou, A., Chappellaz, J., et al. (2012). Carbon isotope constraints on the deglacial CO_2 rise from ice cores. *Science*, *336*(6082), 711–714. https://doi.org/10.1126/science.1217161

Schneider-Mor, A., Yam, R., Bianchi, C., Kunz-Pirrung, M., Gersonde, R., & Shemesh, A. (2005). Diatom stable isotopes, sea ice presence and sea surface temperature records of the past 640 ka in the Atlantic sector of the Southern Ocean. *Geophysical Research Letters*, *32*, L10704. https://doi.org/10.1029/2005GL022543

Seidel, M., & Hlawitschka, M. (2015). An R-based function for modeling of end member compositions. *Mathematical Geosciences*, *47*(8), 995–1007. https://doi.org/10.1007/s11004-015-9609-7

Shakun, J. D., Clark, P. U., He, F., Marcott, S. A., Mix, A. C., Liu, Z., et al. (2012). Global warming preceded by increasing carbon dioxide concentrations during the last deglaciation. *Nature*, *484*(7392), 49–54. https://doi.org/10.1038/nature10915

Sigman, D. M., & Boyle, E. A. (2000). Glacial/interglacial variations in atmospheric carbon dioxide. *Nature*, *407*(6806), 859–869.

Sigman, D. M., Hain, M. P., & Haug, G. H. (2010). The polar ocean and glacial cycles in atmospheric CO_2 concentration. *Nature*, *466*(7302), 47–55. https://doi.org/10.1038/nature09149

Sikes, E. (2012). Radiocarbon in deep water in the Southwest Pacific and Southern ocean since the last glacial maximum. *Quaternary International*, *279–280*, 450–280. https://doi.org/10.1016/j.quaint.2012.08.1482

Sikes, E. L., Elmore, A. C., Allen, K. A., Cook, M. S., & Guilderson, T. P. (2016). Glacial water mass structure and rapid delta-18O and delta-13C changes during the last glacial termination in the Southwest Pacific. *Earth and Planetary Science Letters*, *456*, 87–97. https://doi.org/10.1016/j.epsl.2016.09.043

Skinner, L. C., Fallon, S., Waelbroeck, C., Michel, E., & Barker, S. (2010). Ventilation of the deep southern ocean and deglacial CO_2 rise. *Science*, *328*(5982), 1147–1151. https://doi.org/10.1126/science.1183627

Smith, N. R., Zhaoqian, D., Kerry, K. R., & Wright, S. (1984). Water masses and circulation in the region of Prydz Bay, Antarctica. *Deep Sea Research Part A: Oceanographic Research Papers*, *31*(9), 1121–1147.

Spinrad, R. W., & Zaneveld, J. R. V. (1982). An analysis of the optical-features of the near-bottom and bottom nepheloid layers in the area of the Scotian rise. *Journal of Geophysical Research*, *87*(C12), 9553–9561.

Stephens, B. B., & Keeling, R. F. (2000). The influence of Antarctic sea ice on glacial-interglacial CO_2 variations. *Nature*, *404*(6774), 171–174. https://doi.org/10.1038/35004556

Studer, A. S., Sigman, D. M., Martínez-García, A., Benz, V., Winckler, G., Kuhn, G., et al. (2015). Antarctic Zone nutrient conditions during the last two glacial cycles. *Paleoceanography*, *30*, 845–862. https://doi.org/10.1002/2014PA002745

Stuut, J.-B. W., Prins, M. A., Schneider, R. R., Weltje, G. J., Jansen, J., & Postma, G. (2002). A 300-kyr record of aridity and wind strength in southwestern Africa: Inferences from grain-size distributions of sediments on Walvis Ridge, SE Atlantic. *Marine Geology*, *180*(1–4), 221–233. https://doi.org/10.1016/S0025-3227(01)00215-8

Tang, Z., Shi, X., Zhang, X., Chen, Z., Chen, M.-T., Wang, X., et al. (2016). Deglacial biogenic opal peaks revealing enhanced Southern Ocean upwelling during the last 513 ka. *Quaternary International*, *425*, 445–452. https://doi.org/10.1016/j.quaint.2016.09.020

Theissen, K. M., Dunbar, R. B., Cooper, A. K., Mucciarone, D. A., & Hoffmann, D. (2003). The Pleistocene evolution of the East Antarctic Ice Sheet in the Prydz bay region: Stable isotopic evidence from ODP site 1167. *Global and Planetary Change*, *39*(3–4), 227–256. https://doi.org/10.1016/S0921-8181(03)00118-8

Timmermann, A., Timm, O., Stott, L., & Menviel, L. (2009). The Roles of CO_2 and Orbital Forcing in Driving Southern Hemispheric Temperature Variations during the Last 21 000 yr. *Journal of Climate*, *22*(7), 1626–1640. https://doi.org/10.1175/2008JCLI2161.1

Toggweiler, J. R., Russell, J. L., & Carson, S. R. (2006). Midlatitude westerlies, atmospheric CO_2, and climate change during the ice ages. *Paleoceanography*, *21*, PA2005. https://doi.org/10.1029/2005PA001154

Turekian, K. K., & Wedepohl, K. H. (1961). Distribution of the elements in some major units of the earth's crust. *Geological Society of America Bulletin*, *72*, 175–192.

Vaz, R. A. N., & Lennon, G. W. (1996). Physical oceanography of the Prydz Bay region of Antarctic waters. *Deep-Sea Research Part I: Oceanographic Research Papers*, *43*, 603–641.

Wagner, M., & Hendy, I. L. (2017). Trace metal evidence for a poorly ventilated glacial Southern Ocean. *Quaternary Science Reviews*, *170*, 109–120. https://doi.org/10.1016/j.quascirev.2017.06.014

Watson, A. J., & Naveira Garabato, A. C. (2006). The role of Southern Ocean mixing and upwelling in glacial-interglacial atmospheric CO_2 change. *Tellus Series B*, *58*(1), 73–87.

Wei, G. J., Liu, Y., Li, X. H., Shao, L., & Liang, X. R. (2003). Climatic impact on Al, K, Sc and Ti in marine sediments: Evidence from ODP Site 1144, South China Sea. *Geochemical Journal*, *37*(5), 593–602.

Weltje, G. J. (1997). End-member modeling of compositional data: Numerical-statistical algorithms for solving the explicit mixing problem. *Mathematical Geology*, *29*(4), 503–549.

Whitworth, T., & Orsi, A. (2006). Antarctic Bottom Water production and export by tides in the Ross Sea. *Geophysical Research Letters*, *33*, L12609. https://doi.org/10.1029/2006GL026357

Williams, G., Bindoff, N., Marsland, S., & Rintoul, S. (2008). Formation and export of dense shelf water from the Adélie Depression, East Antarctica. *Journal of Geophysical Research*, *113*, C04039. https://doi.org/10.1029/2007JC004346

Wolff, E. W., Barbante, C., Becagli, S., Bigler, M., Boutron, C. F., Castellano, E., et al. (2010). Changes in environment over the last 800,000 years from chemical analysis of the EPICA Dome C ice core. *Quaternary Science Reviews*, *29*(1–2), 285–295. https://doi.org/10.1016/j.quascirev.2009.06.013

Wolff, E. W., Fischer, H., Fundel, F., Ruth, U., Twarloh, B., Littot, G. C., et al. (2006). Southern Ocean sea-ice extent, productivity and iron flux over the past eight glacial cycles. *Nature*, *440*(7083), 491–496. https://doi.org/10.1038/nature04614

Wu, L., Jing, Z., Riser, S., & Visbeck, M. (2011). Seasonal and spatial variations of Southern Ocean diapycnal mixing from Argo profiling floats. *Nature Geoscience*, *4*(6), 363–366. https://doi.org/10.1038/NGEO1156

Wu, L., Wang, R., Xiao, W., Ge, S., Chen, Z., & Krijgsman, W. (2017). Productivity-climate coupling recorded in Pleistocene sediments off Prydz Bay (East Antarctica). *Palaeogeography, Palaeoclimatology, Palaeoecology*, *485*, 260–270. https://doi.org/10.1016/j.palaeo.2017.06.018

Xiao, W., Frederichs, T., Gersonde, R., Kuhn, G., Esper, O., & Zhang, X. (2016). Constraining the dating of late Quaternary marine sediment records from the Scotia Sea (Southern Ocean). *Quaternary Geochronology*, *31*, 97–118. https://doi.org/10.1016/j.quageo.2015.11.003

Yabuki, T., Suga, T., Hanawa, K., Matsuoka, K., Kiwada, H., & Watanabe, T. (2006). Possible source of the Antarctic bottom water in the Prydz Bay region. *Journal of Oceanography*, *62*(5), 649–655. https://doi.org/10.1007/s10872-006-0083-1